A Composite Cylinder Model for the Prediction of Residual Stresses in Gamma-Titanium Composites

M.S. Al-Haik and H. Garmestani

(Submitted 26 January 2001; in revised form 4 June 2002)

An experimental study of the residual stress formation and evolution in γ-titanium-based composite material was completed for some important processing and heat treatment conditions. A concentric cylinder model based on Norton's creep law with the coefficients replaced by new terms related to time and temperature was developed by a combination of viscoplasticity and thermoelastic analysis of concentric cylinder domains representative for the matrix and the fiber. The x-ray diffraction (XRD) technique was used to measure average residual stresses at the neighborhood of Saphikon fibers. The composite was fabricated by hot isostatic pressing. The residual stress at the matrix decreased as the temperature of the heat treatment increased up to an optimum value, after which the residual stress started to build up despite the increase in the annealing temperature. This phenomenon was depicted through the numerical model as well as in the XRD.

Keywords gamma titanium composites, residual stresses, Saphikon fibers

1. Introduction

Metal matrix composites (MMCs) with improved mechanical properties at elevated temperature and high strength and moduli have emerged as an important class of materials. The introduction of a wide variety of new fibers such as alumina and Saphikon (alumina is polycrystalline Al_2O_3, whereas Saphikon is a single-crystal monofilament developmental ceramic fiber, α-Al_2O_3 with 100% purity Al_2O_3; Saphikon Inc., Milford, NH), SiC, or Al_2O_3-SiO_2, has made it possible to fabricate reinforced light metal matrix composites. Titanium aluminide (γ-TiAl)-based alloys are potentially very attractive low-density, high-strength materials for use at elevated temperatures. TiAl systems offer great potential for weight saving in the hot sections of jet engines.[1] The higher strength-to-weight ratio of titanium (Ti), coupled with good corrosion resistance and excellent ballistic protection, spurred interest in General Dynamic Land Systems (Sterling Heights, MI) U.S. army constructors, to upscale blow-off panels of the M1 Abrams main battle tank.[2] Like most intermetallics, this TiAl alloy suffers from low ductility and fracture toughness at ambient temperatures. Saphikon is thermodynamically stable in TiAl, and its coefficient of thermal expansion closely matches that of TiAl. Observations revealing Saphikon as a good potential reinforcement in TiAl were discussed in Ref. 3.

The processing of MMCs requires that the matrix and the reinforcement material be brought together at elevated temperature followed by cooling to room temperature. Because of a mismatch in the coefficients of thermal expansion between the matrix and fibers, changes in temperature produce residual stresses in the composite. These thermal stresses may be partially relaxed by the plastic deformation of the ductile matrix and lead to additional hardening of the matrix in the composite. Because thermal effects are induced before mechanical testing, their presence can induce the asymmetry in the tensile and compressive yield stresses of the composite.[4]

Because of its influence on the properties of the composite, residual stresses have been the subject of numerous experimental and theoretical studies. Several analyses of residual stresses have been carried out, both experimentally using x-ray diffraction (XRD)[5,6] and neutron diffraction,[7,8] and theoretically by computer simulation. Most of the theoretical works are based on the Eshelby model.[9] This method was introduced in the early 1960s and has since then been successfully applied by numerous researchers to two-phase systems. Finite element modeling emerged as an appropriate technique to predict the residual stress state in MMCs. This approach was used by Rangswamy et al.[7] to predict the residual stress in Ti matrix composite.

Practically, all of the measurements of the residual stresses have been made at room temperature. Because many MMCs are intended for service at elevated temperatures, the residual stresses and their change during typical service conditions at elevated temperatures need to be investigated. In-service thermal cycling may change the residual stress state and thus influence the performance of a component made from MMC materials. Despite the literature describing modeling the fiber-matrix interphase, little was reported about minimizing the residual thermal stresses in MMC materials through different time-temperature cycles, which is the issue addressed in this article.

M.S. Al-Haik, Department of Mechanical Engineering, FAMU-FSU College of Engineering, Florida A&M University, Florida State University, Tallahassee, FL 32316; and **H. Garmestani,** Department of Mechanical Engineering, FAMU-FSU College of Engineering, Florida A&M University, Florida State University, Tallahassee, FL 32316 and Center for Materials Research and Technology (MARTECH), Florida State University, Tallahassee, FL 32316. Contact e-mail: garm@eng.fsu.edu.

2. Theoretical Analysis

Some of the early approaches to study the response of composite materials at the micromechanics level were based on classic elastic-plastic solutions. The elasticity formulation for a variety of loading conditions on solid and hollow cylinders for an isotropic material was established by the previous work of St. Venant.[10] The anisotropic elasticity solution was demonstrated by Avery et al.[11] Theoretical investigation of the stress in a long, hollow, circular cylinder subjected to rapid cooling of the exterior surface was carried out by Jahanian et al.,[12] where a quasi-static uncoupled thermoplastic analysis based on incremental theory of plasticity was developed and a numerical procedure for successive approximation was formulated. The authors assumed that the material had temperature dependent properties and was characterized by linear strain hardening.

The concentric cylinder assemblage model was proposed by Hashin and Rosen.[13] In this model, a unidirectional continuous fiber composite is represented by an assemblage of concentric cylinders, each consisting of a fiber core surrounded by a matrix annulus. The composite cylinder assemblage model was chosen for this study because of its ability to predict effective composite properties by analyzing a single composite cylinder rather than studying the details of the stress at the fiber-matrix interface.

In this model a composite is considered to be an assemblage of composite cylinders. Each cylinder is composed of a circular fiber of radius (a) surrounded by a matrix annulus of radius (b), and the volume of the composite is filled with these composite cylinders, such that each one has the same ratio $(a/b)^2$. This ratio represents the volume fraction of fibers in the composite, such that the entire volume of the composite is filled with nonoverlapping composite cylinders.[14] In the proposed model, two infinitely long concentric cylinders simulate the continuous fiber composite. A cylindrical coordinate system (r, θ, z) is assumed, with z as the axial coordinate and $r - \theta$ as the transverse plane. The initial uniform temperature of the cylinder is assumed to be T_o, which is below the phase transition temperature. In addition, it is assumed that the body forces and the surface tractions are absent. The composite is assumed to be unidirectional with continuous fibers, the fiber is linearly viscoelastic and the matrix is elastic-viscoplastic, the temperature change is uniform in all the phases, and the bonding between phases is perfect. The analysis presented here is based on the work of Mendelson,[15] Jahanian,[12] Jayaraman,[16] and Fabney.[17]

For the proposed composite cylinder model shown in Fig. 1, it is appropriate to assume a plane strain condition $\varepsilon_z = 0$, together with the Tresca criterion and its associated flow rule. It will be assumed that $\sigma_\theta > \sigma_z > \sigma_r$.[15]

The following dimensionless quantities are defined:

$$S_r = \frac{\sigma_r}{\sigma_o}, S_\theta = \frac{\sigma_\theta}{\sigma_o}, S_z = \frac{\sigma_z}{\sigma_o}, S = S_\theta - S_r$$

$$\rho = \frac{r}{a}, \beta = \frac{b}{a}, \tau = \frac{E\alpha T_o}{(1+\nu)\sigma_o} \quad \text{(Eq 1)}$$

where a and b are the internal and external radii for the eccentric cylinder; E is the elastic modulus; σ_o and ε_o are the yield stress and strain of the matrix, respectively; and α is the coefficient of thermal expansion.

Tresca yield criterion for the plane strain assumption will be

$$S = S_\theta - S_r = 1.0 \quad \text{(Eq 2)}$$

Norton's law is chosen here as the constitutive law that correlates the stresses and the corresponding plastic strain rates in the creeping matrix as a function of time and temperature

$$\frac{d\varepsilon^p}{dt} = K_c(\bar{\sigma})^n \exp\frac{-Q}{RT} \Rightarrow \Delta\varepsilon^p = BS^n\Delta t \quad \text{(Eq 3)}$$

where K_c is the creep rate/h, n is the creep exponent, Q is activation energy kJ/mol, R is the gas constant, and T is the absolute temperature in K°. For simplicity, the variable B accounts for the term $K_c \exp(-Q/RT)$. The boundary conditions had been introduced in the model by taking both a stress-free outer surface, and a prescribed displacement and radial stress at the interface as imposed by the fiber and matrix coefficients of thermal expansion α_f and α_m, respectively. By eliminating ε_z and using the dimensionless stress-strain quantities, the equilibrium equation can be written as

$$\frac{dS}{d\rho} + 2(1-\nu)\frac{S}{\rho} - \frac{1}{\nu(\nu+1)}\left(\frac{d\varepsilon_\theta}{d\rho} - 2\frac{\varepsilon_r^p}{\rho}\right) = 0 \quad \text{(Eq 4)}$$

Taking the derivative of Eq 4 with respect to time

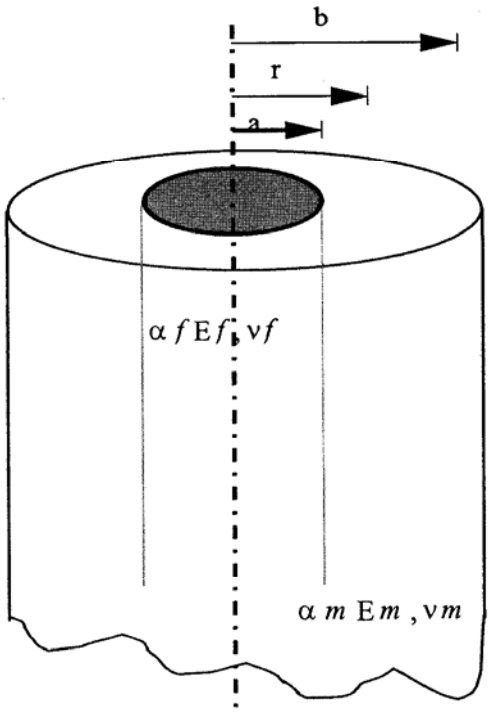

Fig. 1 Concentric cylinder model

$$\dot{\varepsilon}_r^p = \dot{B}\, n\, \dot{S}\, S^{n-1} \rightarrow \dot{B} = B\, \Delta\, t \qquad \text{(Eq 5)}$$

Substituting Eq 5 into Eq 4, and denoting $dS/d\rho$ by $\dot{S}$

$$\dot{S} + 2(1-\nu)\frac{S}{\rho} = \frac{1}{\nu\,(1+\nu)}\left(\dot{B}n\dot{S}S^{n-1}\,\Delta t + 2\frac{\dot{B}S^n\Delta t}{\rho}\right) \qquad \text{(Eq 6)}$$

Let $\ddot{B} = \{(2\dot{B}\Delta t)/[\nu(1+\nu)]\}$, then Eq 6 can be simplified as

$$\dot{S}(1 - \ddot{B}nS^{n-1}) = \frac{2}{\rho}[(1-\nu)S - \ddot{B}S^n)] \qquad \text{(Eq 7)}$$

Introducing new terms

$$\Gamma_0 = \ddot{B}S^n - \frac{2(1-\nu)}{\rho}S \rightarrow \frac{d\Gamma}{dS} = n\ddot{B}S^{n-1} - 2\frac{(1-\nu)}{\rho} \qquad \text{(Eq 8)}$$

Let $\Gamma_0 = BS_0^n - S_0$, where S_0 is the initial normalized stress

$$(1-\nu)\,S = \ddot{B}S_0^n - \Gamma_0\left(\frac{\rho_0}{\rho}\right)^2 \qquad \text{(Eq 9)}$$

Then, for elastic solution (at the fiber domain) $\ddot{B} = 0$ and $\Gamma_0 = S_0$, and

$$S_e = S_0\left(\frac{\rho_0}{\rho}\right)^2 \qquad \text{(Eq 10)}$$

where S_e is the elastic part of the total normalized stress; $S = S_e + S_0$. Initially $S_0 << S_e$ so we can assume

$$S = S_e \quad \text{given that: } S_0 \approx \ddot{B}S_e^n \qquad \text{(Eq 11)}$$

Applying this approximation to Eq 9

$$S \cong \frac{1}{1-\nu}\left[-\Gamma_0\left(\frac{\rho_0}{\rho}\right)^2 + \ddot{B}S_e^n\left(\frac{\rho_0}{\rho}\right)^{2n}\right] \qquad \text{(Eq 12)}$$

Or in a differential form

$$dS_r = \frac{1}{1-\nu}[-\Gamma_0\rho_0^2\rho^{-3} + \ddot{B}S_0^n\rho_0^{2n}\rho^{-2n-1}]\,d\,\rho \qquad \text{(Eq 13)}$$

Solving this ordinary differential equation with the boundary condition: $S_r(\rho)_{\rho\rightarrow\infty} = 0$,

$$S_r(\rho) = \frac{1}{2(1-\nu)}\left[\Gamma_0\left(\frac{\rho_0}{\rho}\right)^2 - \ddot{B}S_0^n\left(\frac{\rho_0}{\rho}\right)^{2n}\right] \qquad \text{(Eq 14)}$$

Similarly, for S_θ

$$S_\theta(\rho) = \frac{1}{2(1-\nu)}\left[\Gamma_0\left(\frac{\rho_0}{\rho}\right)^2 + \left(1 - \frac{1}{2n}\right)\ddot{B}S_0^n\left(\frac{\rho_0}{\rho}\right)^{2n}\right] \qquad \text{(Eq 15)}$$

The set of Eq 14 and 15 was used to calculate the residual stress for the composite after thermal cycling for the desired time periods. Both time and temperature were incorporated in this model via the terms Γ_0 and $\ddot{B}$.

The properties of the Saphikon fibers were provided by the manufacturer (Saphikon Inc., through McDonnell Douglas). However, because this is a developmental fiber, the properties vary according to the filament size and purity of Al_2O_3, as listed in Ref. 18. The γ-TiAl properties are referenced by Kim.[19] Some parameters were measured (radius of fiber) and others were proposed for modeling (Norton's exponent). A summary of the materials parameters used for the simulation is provided in Table 1.

3. Materials and Experimental

A Ti-47Al-2Ta matrix composite reinforced with Saphikon was used in this investigation. The Saphikon fibers had an average diameter of 184 μm. The composite material was fabricated at the McDonnell Douglas Research Center using hot isostatic pressing of powdered matrix material over the different fiber types. Prealloyed Ti-47Al-2Ta powders were milled. All powder handling and milling operations were carried out in argon glove boxes and Ti-lined vials to minimize contamination. No process control agents were used in any milling operation to remove this source of interstitial contamination. Because of the large quantities of powder milled, this material was sealed in Ti-3AL-2.5V (wt.%) tube 6.35 mm in diameter. The tube was electron beam welded at one end. The selected fibers were dropped in through the open end and the remaining space filled with a powder of the matrix material. When the tube was full, the other end was electron beam welded and the material was hot isostatically pressed in vacuum and at 1200 °C. The tubes were sectioned into pieces and each piece was encapsulated in quartz for the heat treatment. The composites were heat treated at 593, 815, and 982 °C for 100, 200, and 500 h at each temperature, followed by cooling to room temperature.

The most widely used nondestructive technique for measur-

Table 1 Values of the Parameters Used for Model Simulation

Quantity	Symbol	Value
Outside diameter of cylinder model	b	250 μm
Radius of the fiber	a	184.3 μm
Activation energy for the matrix	Q	310 KJ/mole
Norton's exponent for creep	n	5
Matrix Young's modules	E_m	170 GPa
Fiber Young's modulus	E_f	470 GPa
Matrix Poisson's ratio	v_m	0.3
Fiber Poisson's ratio	v_f	0.4
Matrix thermal expansion coefficient	a_m	10.6×10^{-6}/°C
Fiber thermal expansion coefficient	a_f	9×10^{-6}/°C
Yield stress of the matrix	σ_o	600 MPa

ing residual stress is XRD.[5,6,7,20] This is a well-established method for the determination of residual stresses in polycrystalline materials, producing a very good measure of the stresses on the surface of the material. The method of XRD depends on the interplane spacing. The interplane spacing becomes a gauge length, which is altered proportionally by elastic stresses. The stresses produce an alteration in interplane spacing, which is divided by the original spacing to become an elastic unit strain that can be interpreted in terms of the corresponding stress. When a material is scanned using XRD, the result is a measure of the intensity of the incident beam at each value of angle θ measured between the incident beam and the planes of atoms. The peaks of the intensity 2θ scan indicate the location of certain atomic planes in the material using Bragg's law:

$$m\lambda = 2d \sin \theta$$

where m is called the order of reflection, and is equal to the number of wavelengths in the path difference between rays scattered by the adjacent planes, λ is the wavelength of the radiation, and d is the inter atomic spacing.

The x-ray coordinate system is shown in Fig. 2. The axis S_i defines the surface of the sample, with S_3 normal to this surface. The laboratory axis L_i is defined such that L_3 is normal to the family of planes $\{hkl\}$, the spacing of which is measured by x-rays. L_2 is in the plane defined by S_1 and S_2 and makes an angle ϕ with S_2, whereas S_3 makes angle ψ with L_3.[6]

The fundamental equation of x-ray strain determination is given as[6]

$$(\varepsilon'_{33})_{\phi\psi} = \frac{d_{\phi\psi} - d_0}{d_0} \tag{16}$$

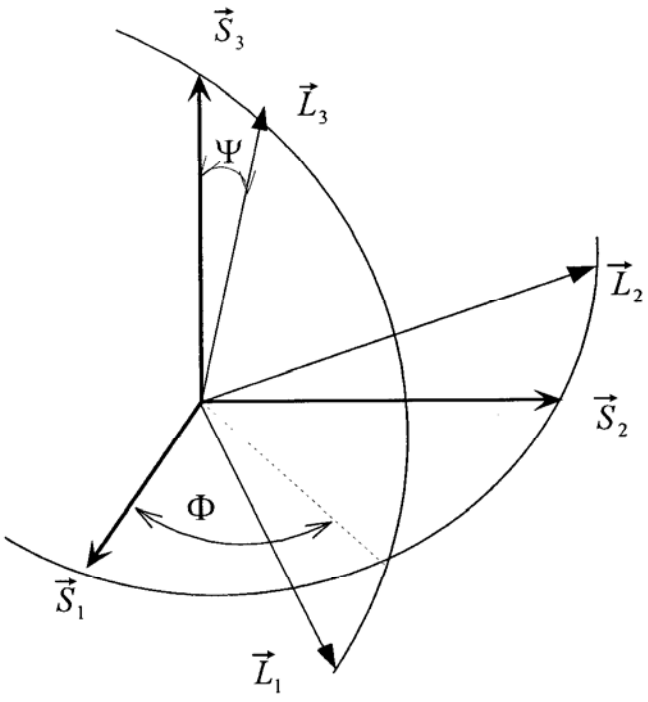

Fig. 2 Definition of the laboratory coordinate system L, sample coordinate system S, and the angles ϕ and ψ

In this equation, $(\varepsilon'_{33})_{\phi\psi}$ is the strain along L_3, $d_{\phi\psi}$ is the lattice spacing obtained from the position of the diffraction peak for a given hkl, and d_o is the unstressed lattice spacing. The angle ϕ is the rotation angle and ψ is the tilt angle.

The strain $\varepsilon'_{33\phi\psi}$ may also be expressed in terms of the strain ε_{ij} in the sample coordinate system by tensor transformation $(\varepsilon'_{33})_{\phi\psi} = A_{3k}A_{3l}A_{kl}$, where A_{3k} and A_{3l} are the direction cosines between L_3 and S_k, S_l respectively. Substituting for A_{3k} in A_{3l},[6]

$$\begin{aligned}(\varepsilon'_{33})_{\phi\psi} = {} & \varepsilon_{11}\cos^2\phi\sin^2\psi + \varepsilon_{12}\sin 2\phi\sin^2\psi \\ & + \varepsilon_{22}\sin^2\phi\sin^2\psi + \varepsilon_{33}\cos^2\psi + \varepsilon_{13}\cos\phi\sin 2\psi \\ & + \varepsilon_{23}\sin\phi\sin 2\psi\end{aligned} \tag{Eq 17}$$

The subscripts 1 and 2 denote strains in the surface plane, whereas 3 indicates strains perpendicular to the surface plane. Equation 17 is a linear equation in six unknowns (ε_{11}, ε_{22}, . . . , ε_{33}) that can be solved by measuring $d_{\phi\psi}$ along six independent directions $(L_{33})_{\phi\psi}$. Following the analysis of Noyan,[6] Dolle,[21,22] and Macherauch,[23] the behavior of d versus $\sin^2\psi$ is observed. Defining the parameters a_1 and a_2

$$\begin{aligned}a_1 &= \frac{d_{\phi\psi+} + d_{\phi\psi-}}{2d_0} - 1 \\ &= (\varepsilon_{11}\cos^2\phi + \varepsilon_{12}\sin 2\phi + \varepsilon_{22}\sin^2\phi - \varepsilon_{33})\sin^2\psi + \varepsilon_{33}\end{aligned}$$

$$\begin{aligned}a_2 &= \frac{d_{\phi\psi+} - d_{\phi\psi-}}{2d_0} \\ &= (\varepsilon_{11}\cos\phi + \varepsilon_{23}\sin\phi)\sin 2|\psi|\end{aligned} \tag{Eq 18}$$

where $\psi_- = -(1)\psi_+$, and $\sin 2\psi_+ - \sin 2\psi_- = 2\sin 2|\psi|$.

The system of Eq 18 predicts a linear variation of a_1 $(\phi\psi)$ versus $\sin^2\psi$ and a_2 $(\phi\psi)$ versus $\sin 2|\psi|$. These data are obtained over a range $\pm\psi$ at three different ϕ angles (0°, 45°, and 90°). The six unknown strains can be obtained by solving the system of Eq 18 at ϕ = 0°, 45°, and 90°. The resulting stresses can then be determined using Hook's law, then the Von Mises effective stress is calculated from the stress components. XRD patterns were obtained using a PW3040 type diffractometer (Philips, Mahwah, NJ) with a PW3050/θ-2θ type goniometer operating at 40 kV and 55 mA.

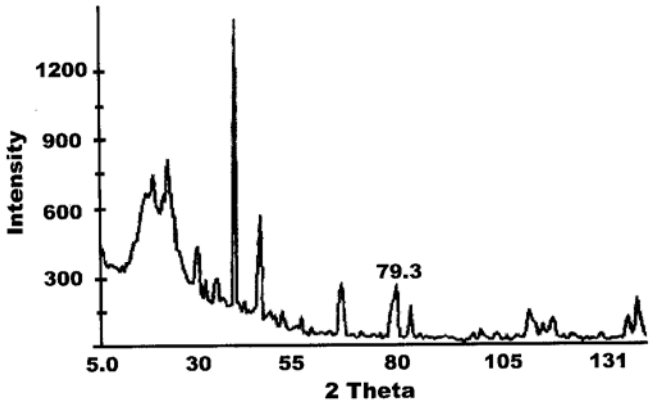

Fig. 3 Diffraction plots for the Ti-47Al-2Ta matrix

4. Results and Discussion

4.1 X-ray Results

Using a 2θ scan, all of the important peaks and their relative intensities were measured for the Ti-47Al-2Ta matrix. From these patterns the unknown interplanar spacing of the crystal planes was determined. The diffractometer is able to measure when 2θ lies between 0° and 150°. An x-ray scan, including all angles that were possible to be measured on the diffractometer, was taken for the Ti-47Al-2Ta matrix to determine the peaks and their relative intensities.

For the calculation of residual stress, the measurements of the interplanar spacing d should be taken at a peak with relatively high angle and a well-defined peak. From Fig. 3, it is clear that the peak at 79.3°, representing the plane [311] in the γ-phase of the material, fits these criteria. The peaks with a greater 2θ values lack both the high intensity and the well-defined peak. The selected peak is known to exist in titanium aluminide. To determine all components of stress, nine angles of ψ (0°, ±15.34°, ±21.97°, ±27.34°, and ±32.01°) were measured at each of three angles of ϕ (0°, 45°, 90°); hence there are 27 pairs of (ϕ,ψ) angles. The d spacing was measured at 27 points (nine values of ψ and three values of ϕ) for each specimen. The six unknown strains can be obtained by solving the following set of equations,[16]

$$a_1(\phi,\psi=0)=\varepsilon_{33},\ a_1(\phi=0,\psi)=\varepsilon_{11}-\varepsilon_{33},\ a_1(\phi=45,\psi)=\frac{1}{2}(\varepsilon_{11}+2\varepsilon_{22}-2\varepsilon_{33})$$

$$a_1(\phi=90,\psi)=\varepsilon_{22}-\varepsilon_{33},\ \frac{a_2(\phi=0,\psi)}{\sin|2\psi|}=\varepsilon_{13},\ \frac{1_2(\phi=90,\psi)}{\sin|2\psi|}=\varepsilon_{23} \quad \text{(Eq 19)}$$

The behavior of a_1 (ϕ,ψ) versus $\sin^2\psi$ is simulated in Fig. 4, whereas a_2 (ϕ,ψ) versus sin|2ψ| is presented in Fig. 5. Both figures are used to find the six unknown strains. Once the strain components are obtained, Hook's law is used to calculate the residual stresses. The resulting Von Mises stresses at different time-temperature cycles are shown in Fig. 6. The error in calculating the effective stress based on the errors within the 2θ angle measurement is calculated to be ~20 MPa.

The residual stress attained its highest value in the hot isostatically pressed sample. The stress of the specimen that was heat treated at 593 °C steadily decreased over the hot isostatically pressed sample residual stress as the time increased. The same trend was observed at 815 °C.

However, at a heat treatment temperature of 982 °C, the stress decreases from the hot isostatically pressed value after 100 h, and then increases slightly with an increase in time. It was observed that the increase in time of heat treatment resulted in a decrease in residual stress up to a transitional temperature, beyond which the stress increases as the duration of heat treatment was increased. For the present analysis, this temperature was estimated between 815 and 982 °C.

4.2. Results of Concentric Cylinder Model

When the thermal stresses are large enough, the matrix will creep. The proposed concentric cylinder model was applied to

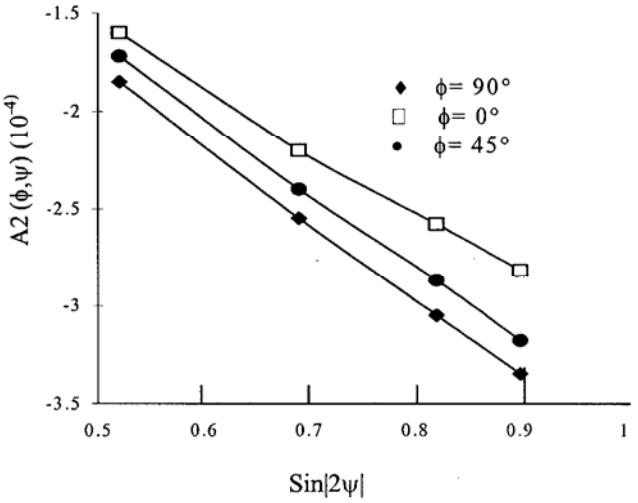

Fig. 5 a_2 (ϕ,ψ) versus sin 2|ψ|. Ti 47Al-2Ta reinforced with Saphikon fiber heat treated at 815 °C for 100 h.

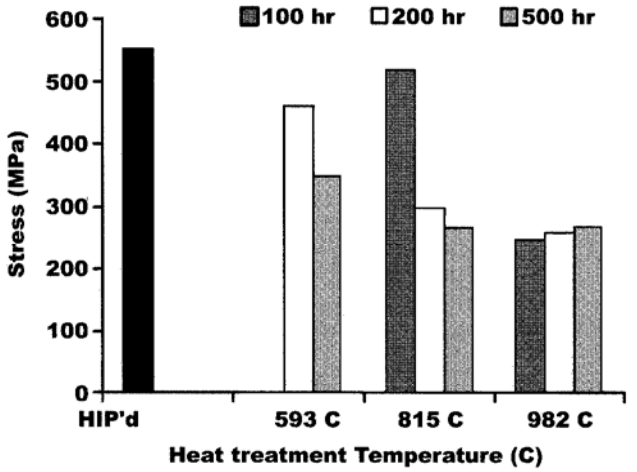

Fig. 6 Von Mises stress measures in Ti-47Al-2Ta reinforced with Saphikon fibers after heat treatment. Results are plotted with as-hot isostatically pressed (HIP'd) sample.

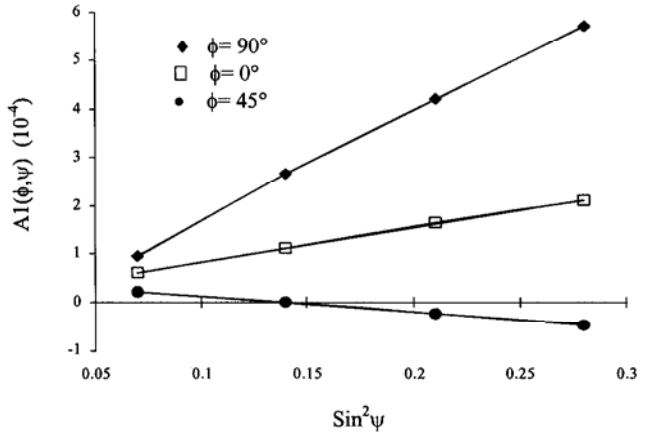

Fig. 4 a_1 (ϕ,ψ) versus $\sin^2\psi$. Ti 47Al-2Ta reinforced with Saphikon fiber heat treated at 815 °C for 100 h.

Saphikon-Ti-47Al-2Ta composite. The materials constants used in the model are presented in Table 1. The initial sample was heated to 1100 °C, then quenched to room temperature. Equations 14 and 15 were used to find the normalized hoop and radial components of the residual stress, respectively. The simulation was done for different cooling rates that were achieved through different time cycles. The effective stress for three different cycles is shown in Fig. 7. If the stress values at each of the temperatures 593, 815, and 983 °C are taken, then Eq 14 and 15 are used for the cooling cycle from each temperature back to room temperature, one obtains the residual stress values after an entire cycle of heating to 1100 °C, then quenching to room temperature, then heating to 593, 815, and 983 °C and then cooling to room temperature at different time cycles.

The results of the final effective stresses after a full cycle for each temperature-time history are simulated in Fig. 8. It is well known that some of the materials parameters will change throughout the temperature range, namely K, Q, and α values. The transient values of those parameters were calculated via extrapolation at different temperatures. Using Norton's creep law with power of $n = 5$ produced five different solutions of the ODE in Eq 13. The maximum numerical value of those five solutions was chosen throughout the simulation.

From the results of Fig. 8, the predicted matrix stress throughout the different time-temperature cycles are fairly close to the experimental values obtained by XRD measurements shown in Fig. 6. Similar to the results of Dixon[24] and Ghonem,[25] thermal cycling of a metal matrix composite can change the room-temperature residual stresses from those predicted after processing. Comparing the experimental measurements to the values obtained via the model, the experimental measurements are slightly higher than the predicted values because the set of material constants does not account for either the phase change or matrix cracking, as shown in Fig. 9.

Despite the difference in the values of the residual stress between the experimental measurement and the numerical model, both results share the same trend. That is, large amounts of plastic deformation will result in a relaxation of the residual stress values. The process of heat treatment can complicate the relaxation of the residual stresses by introducing an annealing process in the matrix that in turn results in the decrease in reaching higher stresses upon the cooling part of the cycle. The experimental and simulation results indicate that the heat treatment at higher temperature resulted in a possible decrease in residual stress. However, the residual stress increased as the time of the heat treatment increased. This can be explained in the model by considering the plastic deformation, where an increase in the time interval or temperature will result in higher plastic strain. It was noted from Fig. 6 and 8 that below some transitional temperatures, the residual stress decreased.

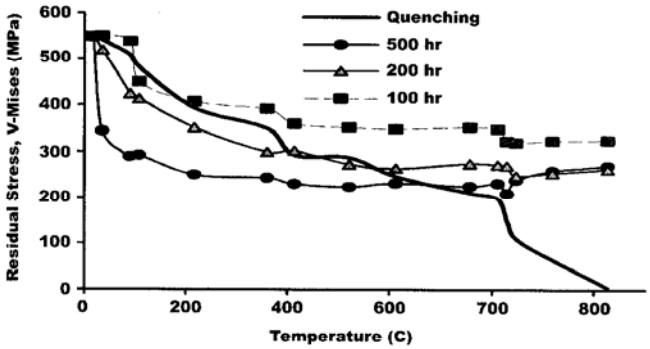

Fig. 7 Effective stress through different time cycles using concentric cylinder model

5. Conclusions

The present analysis shows that a combination of a simple constitutive law (Norton's creep law) with a thermoelastic analysis of a concentric cylinder can yield interesting results even if the detailed material data are not available. The essence of classic viscoplastic behavior that dominates the composite behavior at higher temperature was kept intact. The proposed equation is similar in nature to typical creep power law, but the

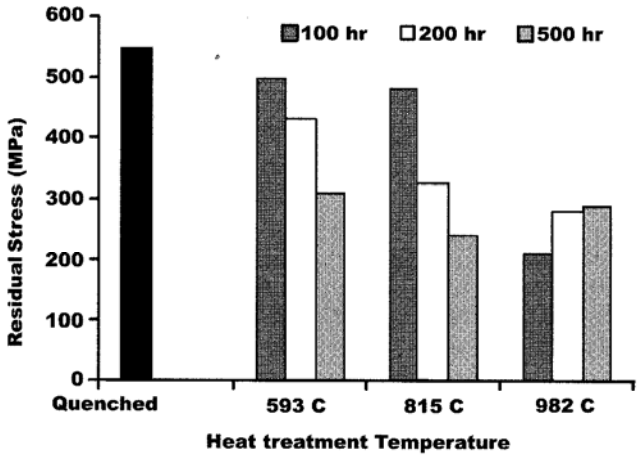

Fig. 8 Effective residual stress for matrix following Eq 14 and 15. The simulation was done for three temperatures at different time periods (cooling rates). Results are plotted with as-hot isostatically pressed sample residual stress.

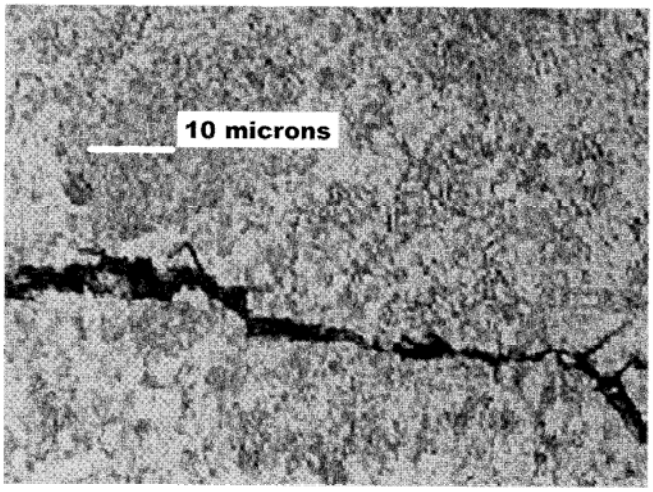

Fig. 9 Microcracks detected in the Ti-47Al-2Ta matrix due to thermal residual stresses

coefficients of this equation have been replaced with expressions involving the time and temperature ratios. The experimental data obtained by XRD showed that the residual stress in the Ti-47Al-2Ta matrix could be adjusted by low-temperature treatment and subsequent reheating to certain temperatures at different time periods (different cooling rates). Hypothetically, with a proper choice of temperature and time combinations, the average residual stresses can be significantly reduced. The proposed model depicted the same trend of the existence of an optimal temperature below which the stress decreases linearly and above which the stress begins to increase again. For the composite used in this study, such an optimal temperature is argued to be in the range 815-982 °C.

Acknowledgment

This work was supported by a grant from the McDonnell Douglas Corporation, St. Louis, MO; NASA/FAMU Center for Nonlinear and Nonequilibrium Aerospace (CENNAS) under Grant No. NCC-252; and the Center for Materials Research and Technology (MARTECH) at Florida State University. The authors would like to thank both Mrs. Catherine Sabinash of McDonell Douglas Corporation and Miss Tyrené A. Townsley from the Mechanical Engineering Department (FSU) for their technical help in preparing the composite samples.

References

1. T. Kelly, P. Bartolotta, J. Barrett, and R. Smashey: "The Use of Ti-48AL-Cr-2Nb in Jet Engines," *J. Met.*, 1997, *49*(5), pp. 48-50.
2. B. Roopchand, J. Montgomery, M.G. Wells, and J. W. Ogilvy: "Low Cost Titanium Armors for Combat Vehicles," *J. Met.*, 1997, *49*(5), pp. 45-47.
3. N. Hoo and P.S. Goodwin: "Microstructural Control in γ- TiAl Alloy by Mn and Hipping." *J. Met.*, 1997, *38*(7), pp. 40-41.
4. G. K. Hu and C.J. Weng: "Influence of Thermal Residual Stress on the Composite Macroscopic Behavior." *Mech. Mater.*, 1998, *27*, pp. 229-40.
5. B.D. Cullity: *Elements of X-Ray Diffraction*, Addison-Wesley, Boston, 1978.
6. I.C. Noyan and J.B. Cohen: *Residual Stress Measurements by Diffraction and Interpretation*, Springer Verlag, New York, 1987, pp. 117-63.
7. M. Daymond, P. Rangaswamy, and M.B. Prime: "Comparison of Residual Strain Measurement by X-ray and Neutron Diffraction in Titanium Matrix Composite," *Mater. Sci. Eng.*, 1999, *A259*, pp. 209-19.
8. D. Kupperman, S. Majumdar, and J. Singh: "Determination of Residual Thermal Stress in SiC-Al2O3 Composite Using Neutron Diffraction," *J. Am. Ceram. Soc.*, 1988, *71*(10), pp. 858-63.
9. J.D. Eshelby: "Elastic Inclusions and Inhomogeneities," *Prog. Solid Mech.* 1961, *2*, pp. 89-140.
10. B. St Venant: "Memoire sur les Divers Generes d'Homogeneite des Corps Solids," *J. Math. Puers Appl.*, 1865, *Ser(II)*, pp. 297-300 (in French).
11. W.B. Avery and C.T. Herakovich: "Effect of Fiber Anisotropy on Thermal Stresses in Fibrous Composites." *J. Appl. Mech.*, 1986, *53*(4), pp. 751-56.
12. S. Jahanian and M. Sabbaghian: "Thermoelastoplastic and Residual Stresses in a Hollow Cylinder With Temperature Dependent Properties," *J. Pressure Vessel Technol.*, 1990, *112*(1), pp. 85-91.
13. Z. Hashin, and B. W. Rosen, "The Elastic Moduli of Fiber Reinforced Materials," *J. App. Mech.* 31, 1964, pp. 223-32.
14. M.W. Hyer: *Stress Analysis of Fiber-Reinforced Composite Materials*, WCB/McGraw-Hill, Boston, 1998.
15. A. Mendelson: *Plasticity: Theory and Applications*, Robert Krieger, Inc., Malabar, FL, 1986.
16. K. Jayaraman and K.L. Reifsnider: "Residual Stress in a Composite With Continuously Varying Young Modulus in Fiber Matrix Interphase," *J. Compos. Mater.*, 1992, *26*(6), pp. 770-91.
17. B. Fabeny and A. Curtin: "Damage-Enhanced Creep and Rupture in Fiber Reinforced Composites," *Acta Mater.*, 1996, *44*(9), pp. 3439-51.
18. Committee on Advanced Fibers for High-Temperature Ceramic Composites, Ceramic Fibers and Coatings: *Advanced Materials for the Twenty-First Century*, National Research Council, Publication NMAB-494, National Academy Press, Washington, DC, 1998, p. 22.
19. Y.W. Kim: "Titanium Aluminides: Aerospace and Automotive Applications" in *The Encyclopedia of Advanced Materials*, Vol. 3, D. Bloor, M.C. Flemings and R.W. Cahn, ed., Cambridge University Press, Cambridge, 1994, pp. 2874-80.
20. A. Weiland and T. Johanesson; "Residual Stresses in Fiber and Whisker Reinforced Aluminum Alloys During Thermal Cycling Measured by X-ray Diffraction," *Mater. Sci. Eng. A*, 1995, *190*, pp. 131-42.
21. H. Dolle and V. Hauk: "Lattice Strains in Coarse Grain Cubic Materials," *Z. Metallkd.*, 1980, *71*(11), pp. 708-13.
22. H. Dolle: "Influence of Multiaxial Stress States, Stress Gradients and Elastic-Anisotropy on the Evaluation of Residual Stresses by X-rays," *J. Appl. Crystallogr.*, 1979, *12*, pp. 489-501.
23. E. Macherauch and U. Wolfstieg: "Recent German Activities in Field of X-ray Stress Analysis," *Mater. Sci. Eng.*, 1977, *30*(1), pp. 1-13.
24. D. Dixon, and J.W. Newkirk: "Gamma Titanium Aluminide Reinforced With Al_2O_3 and TiB_2 Fibers," *Mar. Res. Soc. Symp. Proc. 288*, Materials Research Society, Pittsburgh, PA, 1992, pp. 1063-68.
25. Y. Wen, H. Ghonem, and D. Zheng: "An Interactive Simulation Technique to Determine the Internal Stress in Fiber Reinforced Metal Matrix Composites," *Mater. Sci. Eng. A*, 1994, *177*(1-2), pp. 125-34.